Materials Today Communications 53 (2026) 115313

Contents lists available at ScienceDirect

Materials Today Communications

journal homepage: www.elsevier.com/locate/mtcomm

Metallized thermoplastic nonwovens as integrated heating elements in fiber-reinforced composites

Paulina Latko-Durałek [a,*], Michał Misiak [a], Dola Temesgen Ufaysa [a], Nan Tao [b,*], Bartłomiej Przybyszewski [a], Paweł Durałek [c], Daria Rutkowska [a], Milena Kurkowska [d], Andrei Anisimov [b], Otto Bergsma [b], Roger M. Groves [b], Anna Boczkowska [a]

[a] Faculty of Materials Science and Engineering, Warsaw University of Technology, Woloska 141, Warsaw 02-507, Poland
[b] Department of Aerospace Structures and Materials, Delft University of Technology, Kluyverweg 1, Delft 2629 HS, the Netherlands
[c] Technology Partners Foundation, Bitwy Warszawskiej 1920r. 7A, Warsaw 02-366, Poland
[d] Łukasiewicz – Industrial Chemistry Institute, Rydygiera 8 Str., Warsaw 01-793, Poland

ARTICLE INFO

Keywords:
Metallized nonwoven
Shearography
De-icing
Glass fiber-reinforced polymers

ABSTRACT

This study investigates the multifunctional potential of metallized polyphenylene sulfide (PPS) nonwovens integrated as electrically conductive interlayers in glass fiber-reinforced polymer (GFRP) composites. The PPS nonwovens were coated with a nickel–phosphorus layer via electroless plating and embedded between the laminate plies. The system was evaluated both as an electrothermal heating element for de-icing and as a sensing layer for non-destructive testing. For de-icing applications, icing wind tunnel tests were conducted under glaze-ice and mixed-ice conditions. The integrated heating layer enabled complete ice removal within approximately 120 s for both icing regimes, while the distributed Joule-heating mechanism ensured stable and spatially uniform surface temperatures. Furthermore, the metallized nonwovens were successfully applied as an internal thermal excitation source in shearography, allowing clear identification of impact-induced damage, including delamination. The incorporation of the metallized PPS interlayer also enhanced the mechanical performance of the GFRP composite, with flexural strength increasing from 944 MPa (reference) to approximately 1164 MPa. Dynamic mechanical analysis indicated a slight increase in glass transition temperature from 132 °C to 141 °C. These findings demonstrate that metallized thermoplastic nonwovens provide an effective approach to designing multifunctional composites for advanced engineering applications.

1. Introduction

Nonwoven fabrics are broadly defined as sheet or web structures composed of randomly distributed fibers that are bonded together through mechanical, thermal, or chemical processes. Unlike woven or knitted textiles, nonwovens are produced directly from separate fibers (e.g. in the needle punch process) or molten polymers (e.g. in the melt-blowing process) without the intermediate step of converting fibers into yarns [1]. This direct manufacturing route allows to obtain a rapidly expanding class of fibrous materials to be obtained that combine the versatility of thermoplastic polymers with the structural benefits of nonwoven architectures. Mainly due to their tunable morphology including fiber diameter, pore structure, thickness, and basis weight (grammage, areal density) thermoplastic nonwovens have become essential materials across multiple industrial sectors due to their low weight, mechanical strength, and ability to be thermoformed into complex shapes [2]. In the automotive and construction sectors, thermoplastic nonwovens are widely used for interior components, insulation, roofing membranes, geotextiles, and vapor barriers due to their durability and weather resistance. They are also essential in medical, hygiene, and filtration products, providing controlled porosity, chemical resistance, and cost-effective mass production. Beyond traditional uses, thermoplastic nonwovens are also used in the composite sector as reinforcement layers, providing improved tensile strength, impact resistance, and dimensional stability. Additionally, nonwovens are employed as surface veils or interlayers to enhance surface quality and toughness [3].

Advances in polymer engineering and fiber processing have greatly expanded the functional potential of thermoplastic nonwovens. The ability to incorporate additives, nanofillers, or surface treatments allows

* Corresponding authors.
E-mail addresses: paulina.latko@pw.edu.pl (P. Latko-Durałek), n.tao@tudelft.nl (N. Tao).

https://doi.org/10.1016/j.mtcomm.2026.115313
Received 2 February 2026; Received in revised form 25 April 2026; Accepted 30 April 2026
Available online 1 May 2026

for the fine-tuning of mechanical, thermal, electrical, and barrier properties [4–6]. One of the approaches to make nonwovens functional is applying the metallization process to create on their surface metallized layer typically from aluminum, copper or nickel. Nonwoven structures, characterized by their high surface area, tunable porosity, and versatile fiber architectures, provide an ideal substrate for metallization processes such as electroless plating, physical vapor deposition, sputtering, or solution-based metallization [7,8]. Metallizing nonwovens based on thermoplastic polymers, for instance polypropylene (PP), polyesters, polyamides (PA), or high-performance matrices like polyimide (PI) enables the creation of hybrid systems that retain the inherent advantages of the polymer, mainly light weight, flexibility and recyclability with added electrical or thermal functionalities [9–11]. When integrated into fiber-reinforced polymers, metallized nonwovens can be used as a shielding layer against electromagnetic interference (EMI) or for enhanced thermal management [12,13]. These hybrid systems enable the development of multifunctional composites for applications in aerospace, automotive, electronics, and defense, where both structural performance and functional capabilities are required.

In this paper, the use of metallized polyphenylene sulfide (PPS) nonwovens as an electrically conductive layer integrated into glass fiber-reinforced polymers (GFRP) is presented, highlighting their multifunctional capabilities. Their performance is evaluated both as a heating element for electrothermal de-icing and as a sensing layer in shearography NDT (non-destructive testing) methods, while also considering the effect of metallized nonwovens on the mechanical properties of the composites. To the best of the authors' knowledge, such a comprehensive study combining these functionalities has not been reported previously.

Active anti-icing systems are increasingly employed in aerospace and wind energy applications to ensure operational safety and maintain aerodynamic performance under icing conditions [14]. Ice accretion on lifting surfaces or rotating blades alters local flow characteristics, reduces lift, increases drag, and can ultimately lead to structural or functional failure. Conventional de-icing methods include mechanical removal, chemical treatments, and thermal techniques. Mechanical methods rely on scraping or brushing ice from surfaces, while chemical approaches use salts or glycol-based solutions to melt or prevent ice formation. Thermal de-icing, increasingly employed in advanced composites, utilizes resistive heating or embedded conductive layers to efficiently remove ice [15,16]. For instance, the Boeing 787 employs a metal-sprayed electric heating element inserted between multi-layer carbon fiber-reinforced polymer (CFRP) laminates, creating an electric heating icing protection system [17]. However, such methods are often unsuitable for fiber-reinforced polymers due to limited flexibility and low efficiency. New solutions based on the electrothermal de-icing process involve the use of electrically conductive materials or elements to generate heat through the Joule effect, melting ice or preventing its accumulation on surfaces. In this process, an electric current passes through a conductive layer such as a carbon-fiber fabric, or embedded conductive film which converts electrical energy into heat [18]. The generated thermal energy raises the surface temperature above the freezing point of water, effectively removing ice or preventing its formation. In particular, solutions based on thermoplastic matrices containing electrically conductive fillers exhibit stable electrical conductivity, tunable thermal output, and compatibility with standard composite manufacturing techniques [19]. Unlike metallic heating foils or wires, thermoplastic polymers with conductive fillers can be applied consistently over complex geometries without increasing the overall weight, and eliminate stress concentrations associated with stiffness mismatches [20]. Moreover, in the case of thermoplastic nonwovens, the heating patterns arising from the fiber distribution promote more uniform surface temperature control, potentially improving energy efficiency and reducing power input requirements during de-icing or anti-icing operations [21]. These advantages position metallized PPS-nonwovens as highly adaptable heating elements for composite structures such as GFRPs. Therefore, demonstrating their performance under different icing conditions is essential to assess their applicability as an integrated, low-energy active de-icing technology.

In the aerospace sector, GFRP composites are commonly used at the leading edge of the tail and at the wings. Those composite structures are susceptible to impact damage from hail, bird or tools, which may significantly affect structural integrity and safety [22]. Therefore it is important to advance non-destructive testing techniques towards timely inspection and monitoring of composite aircraft structures. Among the various kinds of NDT techniques, shearography is an optical method that can measure surface strain under structural loadings [23,24]. It reveals defects by finding defect-induced surface strain anomalies. A certain loading is needed for shearography inspection, such as thermal or mechanical loadings [25]. The outputs from shearography include fringe and phase maps, which can be related to surface strain components of the test structure. Shearography can be used for the structural inspection of aerospace and marine composite structures [26] and recent developments have enabled the detection of deep or submilimeter defects [27] as well as the inspection of curved objectives [28].

2. Materials and methods

2.1. Metallization process of PPS nonwovens

In this work, thermoplastic polyphenylene sulfide (PPS) nonwovens having an areal weight of 60 g/m^2 were coated by a nickel-phosphorus (Ni-P) electroless plating process. Three pieces of nonwoven with dimensions of 12 × 12 cm were used for composite sample preparation. One of the nonwoven samples remains as a reference and the remaining two samples go through the metallization process. Fig. 1 shows a metalization process scheme. The nonwoven samples were first cleaned and degreased in 300 mL acetone for 5 min and rinsed with distilled water for additional 5 min. Sensitization of nonwoven surface was performed by immersing the samples in 300 mL $SnCl_2$/HCl aqueous solution for 10 min, followed by a 5-minute distilled water rinse. To perform activation, the samples were placed in 300 mL $PdCl_2$/HCl aqueous solution for 5 min, enabling the reaction $Sn^{2+} + Pd^{2+} \rightarrow Sn^{4+} + Pd^0$, and then rinsing again for 5 min. The activated samples underwent electroless Ni-P plating in a deposition bath for 15 min. Both the bathes were preheated to 80 °C for 20 min to ensure appropriate conditions for deposition (deposition rate, grain size, crystallinity, etc.). The Ni-P plated samples were rinsed twice with distilled water for 10 min each and air-dried under clean conditions. Fig. 2 shows the appearance of the PPS nonwoven before(a) and after(b) the metallization process.

2.2. GFRP fabrication

GFRP laminates were manufactured using HexPly® M9.6GF/32%/UD1200/G unidirectional epoxy–glass prepreg containing 32 wt% of the M9.6GF epoxy resin system and 1200 g/m^2 E-glass fibers, supplied by Hexcel, USA, which provides stable handling at room temperature and allows for consistent processing under vacuum. Each laminate consisted of 8 plies of glass fiber prepreg, and in the modified variant, a metallised nonwoven layer intended to function as an integrated heating element was introduced between the 2nd and 3rd plies. The laminate therefore consisted of 8 plies of prepreg and one metallized PPS nonwoven interlayer, resulting in a total thickness of approximately 3.5 mm after consolidation. The placement position was determined through repeated experiments at various locations to obtain optimal performance. This placement ensured both mechanical protection of the heating layer and effective thermal coupling to the surrounding matrix. The laminates were produced by vacuum bagging at −0.9 bar, a pressure sufficient to consolidate the plies and ensure uniform integration of the embedded layer. They were then cured in an SPT-200 vacuum dryer at 100 °C for 1 h. After curing, the panels were demolded, trimmed, and visually inspected to verify proper consolidation and the absence of

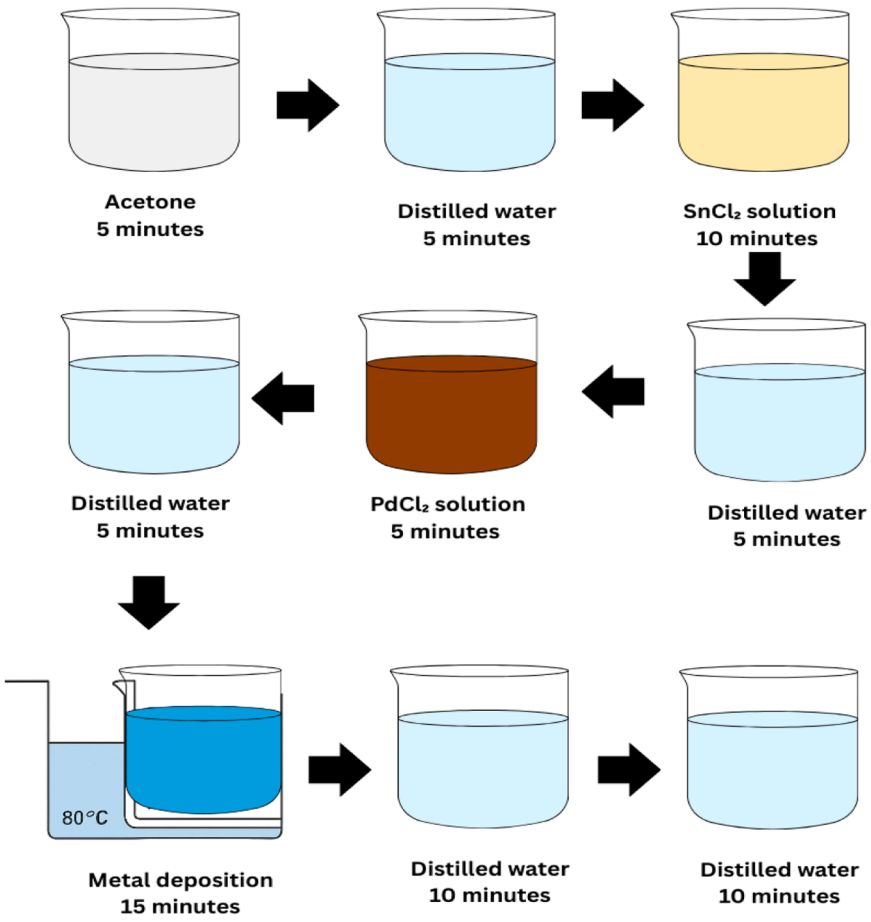

Fig. 1. Schematic representation of the metallization process of PPS nonwovens.

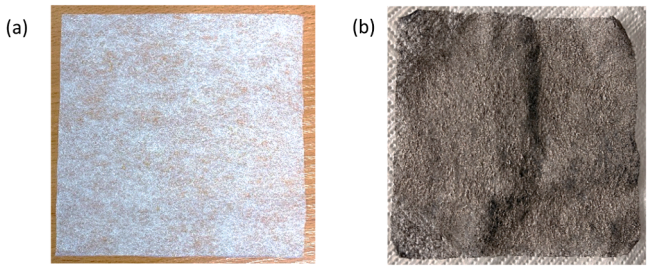

Fig. 2. PPS-nonwoven before (a) and after (b) metallization process.

defects, such as local delamination around the metallised interlayer. The applied procedure yielded two materials: a reference laminate composed solely of prepreg plies and a modified laminate containing the fully embedded metallized PPS-nonwoven layer, which was subsequently used for mechanical and functional characterisation.

2.3. Characterization of metallized PPS-nonwovens

The surface morphology of the nonwoven samples was examined using a Hitachi TM3000 Scanning Electron Microscope (Hitachi, Japan) to assess both the quality and uniformity of the electroless nickel–phosphorus (Ni–P) coating. SEM observations were performed on the metallized nonwovens at an accelerating voltage of 15 kV in backscattered electron (BSE) mode.

The PPS-nonwovens after the metallization process were also characterized using a JEOL JSM-7600F field-emission Scanning Electron Microscope equipped with energy dispersive X-ray spectrometer (EDS) for elemental analysis. SEM observations were performed in LEI mode at an accelerating voltage of 5 kV and a magnification of 500x and 1000x.

The multimeter probes were connected to copper tape applied to two opposite corners of each nonwoven sample to ensure reliable electrical contact. Measurements were taken at the top, middle, and bottom regions of each sample to verify the uniformity of the conductive coating. The metallized samples were then cut into 10 cm × 10 cm specimens, with copper tape applied at both ends to ensure effective electrical connections. Each sample was placed on a thermally insulating substrate, connected to a DC power supply, and subjected to applied voltages of 5, 10, and 15 V. The resulting thermal response was recorded over a period of 60 s using a FLIR TG267 infrared camera.

2.4. Characterization of GFRP composites with metallized nonwovens

2.4.1. Microstructure of GFRP panels

The SEM (TM3000, Hitachi, Japan) was used to investigate the quality of the GFRP composite's microstructure especially after implementation of metallized nonwovens. The cross-sections of the GFRP samples, first embedded and cured in resin, were sequentially polished using a Motopol 2000 polisher (Buehler, USA) with sandpapers of increasing grit sizes: 800 → 1200 → 2500 → 4000. The polished surfaces were coated with a conductive gold sputter layer. The SEM was operated at an accelerating voltage of 15 kV in backscattered electron (BSE) mode, and each sample was examined at four magnification levels: 50 × , 100 × , 150 × , and 200 × .

2.4.2. De-icing test of GFRP composites with metallized nonwovens

The icing experiments were conducted in an open icing wind tunnel operated by the Technology Partners Foundation (Warsaw, Poland)

[29]. The facility enables controlled reproduction of in-flight icing conditions through simultaneous regulation of airflow velocity, spray droplet characteristics, temperature, and liquid water content (LWC). For the present study, the test section was operated at an airspeed of 20 m/s, with an LWC of 0.5 g/m^3 and a median volume diameter of 30 μm, generated by a pressurized water atomization system (Spraying Systems Co, Deinze, Belgium). The water and air supply pressures were set both to 1 bar, to achieve the desired droplet distribution. Two icing regimes were examined: glaze ice formed at −5 °C and mixed ice formed at −10 °C, while maintaining identical hydrodynamic spray conditions. The GFRP specimen containing the embedded metallized PPS- heating nonwoven was mounted horizontally in the centre of the test section, with its surface inclined at an angle of 135° relative to the spray nozzle, ensuring uniform exposure to the droplet-laden flow. Prior to activation of the heating system, each specimen was subjected to spray for 5 min to allow the formation of a representative ice layer. Following ice accretion, the spray was halted while the airflow and temperature were maintained, and the heating element was energized using a DC power supply SP Series 1 CH DC (Owon, Hong Kong). The electrical leads were connected to copper tape electrodes (12 mm width) applied along the edges of the metallized nonwoven layer, with an overlap of approximately 6 mm to ensure reliable electrical contact. The electrical connections to the DC power supply were made at the ends of the electrodes. The supply voltage was set to 30 V, resulting in a current draw of 0.7 A. The de-icing behaviour was monitored from the moment of power activation until complete melting of the accumulated ice. The de-icing time was recorded using a synchronized data-acquisition system, while the surface temperature distribution was continuously measured with an infrared camera FLIR 187 66 (Oregon, USA) positioned outside the tunnel and calibrated for the specimen's emissivity. Infrared images were acquired, enabling temporal tracking of the maximum surface temperature. This methodology allowed for qualitative assessment of the thermal performance of the integrated PPS-based heating system under representative glaze and mixed-ice conditions.

2.4.3. Shearography test of GFRP composites with metallized nonwovens

In this work, an out-of-plane shearography instrument [26] was adapted for the damage detection of the GFRP composites with metallized nonwovens. A schematic of the Shearography setup is shown in Fig. 3. In the test, a laser beam is expanded with a beam expander to illuminate the specimen surface. By tilting the shearing device by a small angle, the scattered light from two neighboring positions on the specimen surface interferes at the CCD camera and is recorded as a speckle interferogram. The shearing device allows control of both the shearing amount and shearing direction (e.g., δy in the y-direction in Fig. 3), enabling phase-shifting for obtaining the optical phase of the recorded speckle interferograms. For this study, shearography NDT was performed before and after the impact test of the specimens (impact energy of around 30 J). During the measurement, the bottom edge of the tested specimen was clamped; the specimen was heated by using the embedded metalized PPS-nonwovens for around 240 s (by applying a voltage of 15 V). A shearography camera was used to continuously capture phase-shifted speckle interferograms before heating, during heating, and during natural cooling of the specimen. A phase map for defect detection was obtained by comparing two deformation states of the specimen. Besides, phase compensation can be needed to remove the phase change due to the overall deformation. This can be done by subtracting the original phase map with a fitted surface using polynomial fitting [30]. In principle, the specimen needs to be loaded to detect damage with shearography. A common and convenient method to detect impact-induced subsurface damage with shearography is heating and cooling the sample to apply loading. External heating is normally used; however, the GFRP specimen used in the present study has a self-heating capability. Therefore, it is more convenient to utilize this capability to load the sample.

2.4.4. Mechanical performance of GFRP composites

Three-point bending tests were carried out in accordance with ASTM D7264 using an MTS QTest universal testing machine (MTS Systems Corporation, USA) fitted with a 10 kN load cell. A schematic representation of the three-point bending test setup is shown in Fig. 4.Rectangular specimens measuring approximately 4 × 10 × 80 mm (thickness × width × length) were prepared, with five samples of each material. The tests were performed at a crosshead speed of 1 mm/min, using a support span of 64 mm. Both the loading nose and supports had diameters of 6 mm. During testing, the specimens were positioned such that the metallized PPS nonwoven interlayer was located on the tensile side (lower surface). Flexural modulus (E_f) and flexural strength (σ_{fM}) were calculated from the force–deflection curves following the ASTM D7264 procedure.

Dynamic mechanical analysis (DMA) was employed to characterise the viscoelastic response of the produced GFRP laminates and to

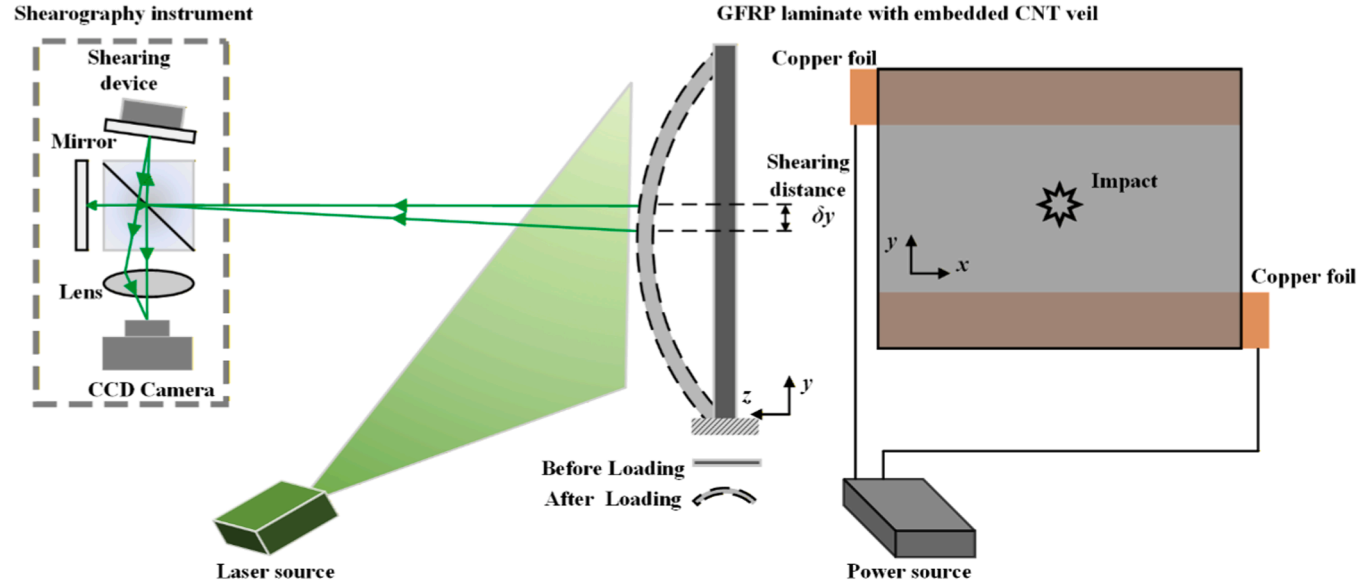

Fig. 3. Diagram of the shearography instrument based on a Michelson interferometer for impact damage detection of the GFRP laminates with embedded metallized nonwovens.

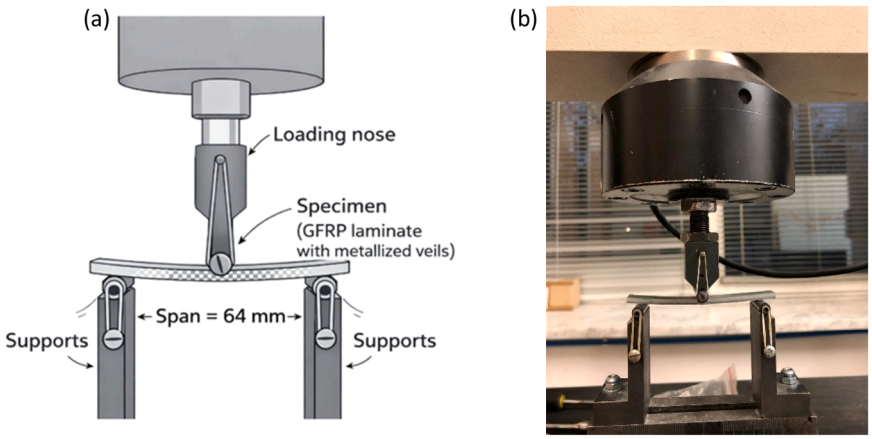

Fig. 4. (a) Schematic representation of the three-point bending test setup and (b) the experimental configuration with a specimen.

examine whether the inclusion of printed conductive paths altered their thermo-mechanical behaviour. Measurements were carried out using a DMA Q800 (TA Instruments, USA) in a dual-cantilever configuration, in accordance with ASTM D7028. Rectangular specimens were subjected to a temperature sweep from 0 to 180 °C at a heating rate of 3 °C/min while oscillated at 1 Hz with a displacement amplitude of 20 μm. The resulting DMA curves were used to determine the glass transition temperature (T_g) and the storage modulus at ambient conditions (E'_{RT}).

3. Results and discussion

3.1. Properties of metallized PPS-nonwovens

The SEM images in Fig. 5 show a nonwoven fiber network which is dense, compact and forms an entangled structure. The images presented in Figs. 5a and 5b are for nonmetallized PPS nonwovens before the Ni-P coating. The metallization process preserves the fibrous structure of the nonwoven material. The individual fibers remain clearly distinguishable and are uniformly coated with a continuous metallic layer which is easily recognized in the images shown in Figs. 5c, 5d and in Figs. 6a and 6b. The deposition results in increased surface roughness, with fine granular features visible along the fiber structure, indicating effective nucleation and growth of the metallic coating. A small number of microcracks can be observed on the coated fiber surfaces. Moreover the thickness of the nonwovens after the metallization process increases from 0.59 ± 0.07 mm to 0.74 ± 0.08 mm. The EDS analysis in Fig. 6c confirms nickel as the dominant element (57.82 wt%), verifying successful metallization of the nonwoven. Oxygen (22.63 wt%) and phosphorus (15.47 wt%) are also detected, which may be associated with surface oxidation and the chemical nature of the deposition layer.

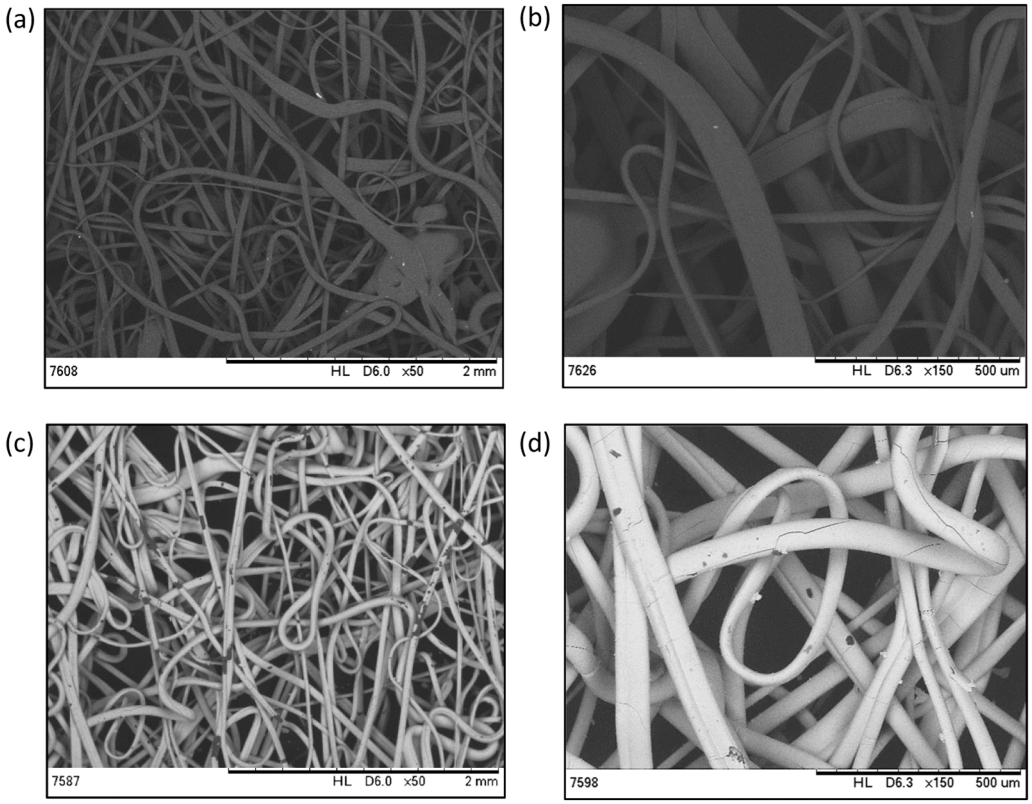

Fig. 5. Microstructure of PPS-nonwoven before (a, b) and after (c, d) metallization process.

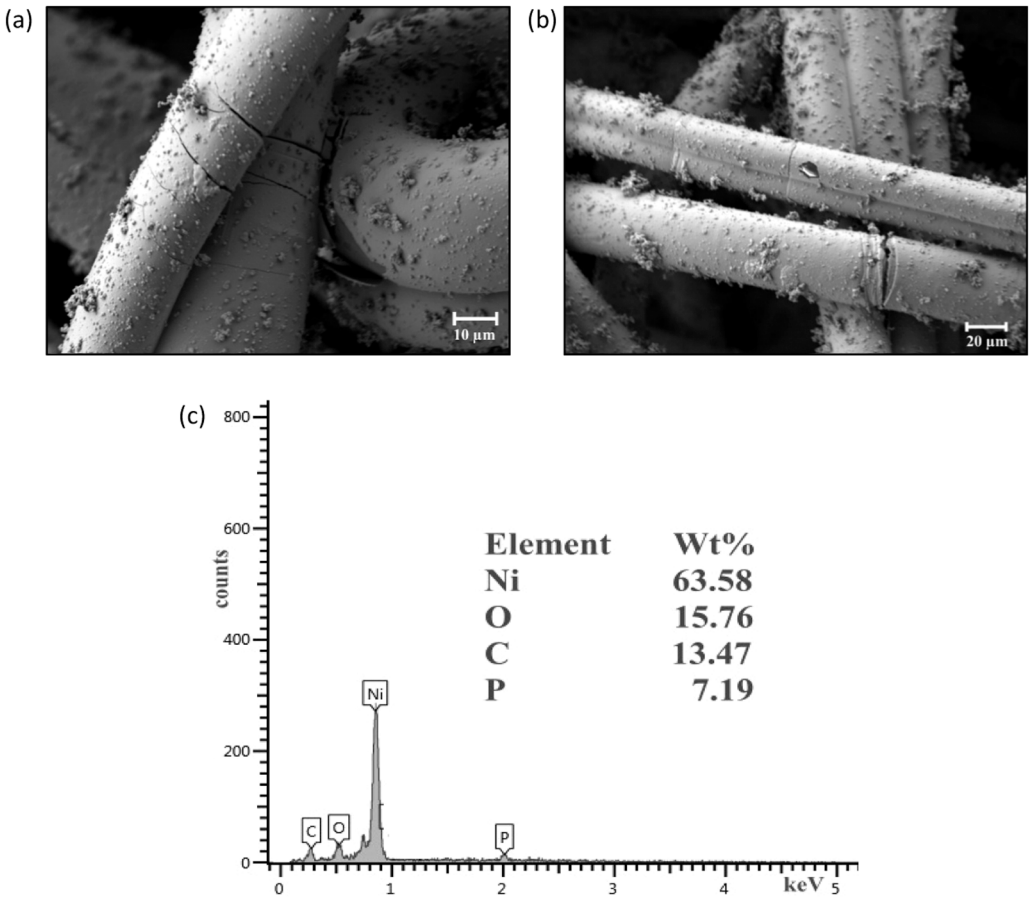

Fig. 6. SEM micrographs (a,b) and EDS analysis (c) of metallized PPS-nonwovens.

The presence of nickel particles in the metallized PPS nonwoven results in excellent electrothermal (Joule heating) performance with a rapid response. The uniform distribution of nickel ensures efficient current flow and heat generation. A key advantage of this system is the ability to precisely control the heating output by adjusting the applied voltage and current, independent of external conditions [10]. The average electrical resistivity of the metallized PPS nonwovens was 1.1 ± 0.18 kΩ. Measurements were performed at three different locations on each sample, and the consistently low resistance values confirmed the formation of a continuous metallic layer across the nonwoven' surface. Under applied voltages of 5, 10, and 15 V, a temperature increase was observed, as shown in infrared thermal images collected in Table 1. Higher applied voltages resulted in greater heat generation due to enhanced Joule heating. The maximum temperature, approaching 30 °C, was reached at 15 V after 60 s. This behavior indicates that the metallized network provides effective electrical conductivity and suggests its potential for applications such as thermal-based damage or delamination sensing in composite systems.

3.2. SEM of GFRP panels

The effect of integrating metallized PPS nonwovens on the quality of GFRP composites is shown in the cross-sectional images of panels in Fig. 7. Overall, the composites exhibit good quality, with no visible defects or delamination. According to the SEM images, the nonwoven interleaf interacts similarly with the adjacent glass fibers across both laminates. The interfaces show no signs of chemical or mechanical changes, indicating that the metallic layers on the nonwovens do not affect their structure. However, it is noticeable that during resin curing, the thermoplastic nonwovens partially melted, forming island-like structures with recognizable metallic layers (appearing white) around them. Resin infiltration was effective in both composites, with the resin filling elongated and irregular voids that formed within the resin-rich bands.

3.3. Ability to use metallized nonwoven for de-icing

Fig. 8 presents the visual condition of the GFRP specimens with the embedded metallized PPS-nonwovens after ice accretion in the icing wind tunnel. Distinct differences between the two icing regimes were observed: the glaze ice generated at −5 °C formed a transparent, smooth surface coating, whereas the mixed ice produced at −10 °C resulted in a more irregular and crystal-like layer due to the partial freezing of supercooled droplets upon impact. These initial surface states represent typical ice morphologies encountered under moderate and colder atmospheric icing conditions, respectively [31,32].

Upon activation of the direct current heating system, rapid melting of the accumulated ice was observed in both regimes. As shown in Fig. 9a, the glaze-ice specimen exhibited complete melting of surface ice within approximately 120 s, with visible water droplets beginning after the first few tens of seconds of heating. A similar outcome was obtained for the mixed-ice specimen (Fig. 9b), although the melting front progressed slowly during the initial phase due to the lower starting temperature of both the environment and the specimen. Nevertheless, full de-icing on the embedded metallized PPS-nonwovens area was also achieved within approximately 120 s, demonstrating that the integrated nonwoven heating layer was capable of delivering sufficient thermal power even under more severe icing conditions.

The temporal evolution of surface temperature, captured using an infrared camera, is presented in Fig. 10 for both icing regimes. For the

Table 1
Infrared thermal images of metallized PPS nonwoven under various voltage and time.

Heating time (s)	Voltage		
	5 v	10 v	15 v
0	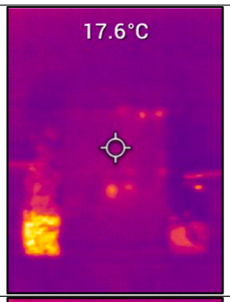	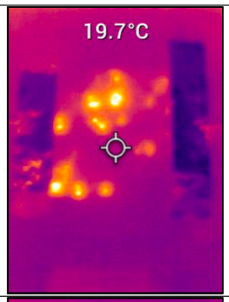	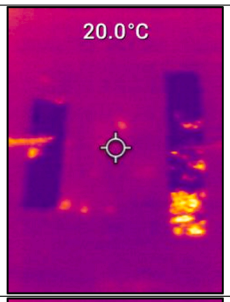
10	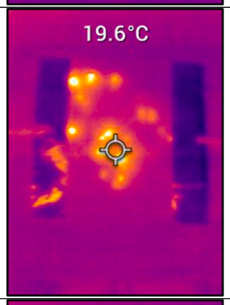	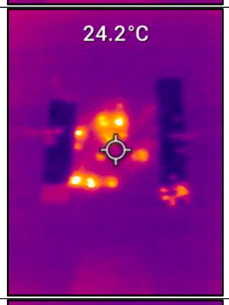	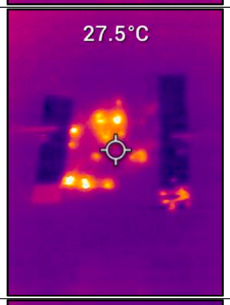
30		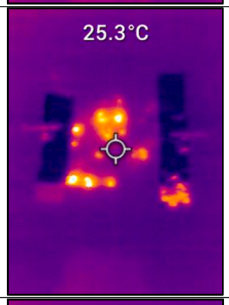	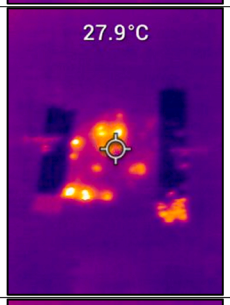
60			

glaze-ice test (Fig. 10a-c), the surface temperature increased rapidly from the initial −5.4 °C at 0 s to 32.6 °C after 30 s, reaching maximum values of 62.4 °C at 120 s.In contrast, the mixed-ice specimen (Fig. 10d-f) exhibited systematically lower temperatures at corresponding time intervals (e.g., 18.9 °C at 30 s and 50.5 °C at 120 s), reflecting the greater thermal losses in the colder tunnel environment and the higher heat flux required to raise the surface above the melting point. Despite this, the temperature distribution remained stable and spatially uniform, confirming the effectiveness of the embedded nonwovens with the metallic coating as a heating layer in maintaining homogeneous thermal output across the composite surface.

The experimental results confirm that electrically conductive metallized nonwovens used as a heating layer integrated into GFRP provides efficient and reliable de-icing performance under representative glaze- and mixed-ice scenarios. The system achieved full ice melting from both surface types within approximately two minutes of activation, without evidence of localized overheating or thermal discontinuities. The distributed nature of the Joule-heating mechanism ensured uniform surface temperatures, while the lower mass and improved structural compatibility of the nonwoven-based heating layer compared with traditional metallic foils or wires offer clear advantages in applications where weight, compatibility, and durability are critical.

3.4. Ability to use metallized nonwoven in shearography

Preliminary experiments were performed to determine whether the introduction of the PPS interlayer itself promoted interfacial debonding between the PPS and GFRP layers. To this end, one GFRP specimen without a PPS layer (Fig. 11a) and one GFRP specimen with a PPS layer (Fig. 11b) were inspected using shearography with thermal loading

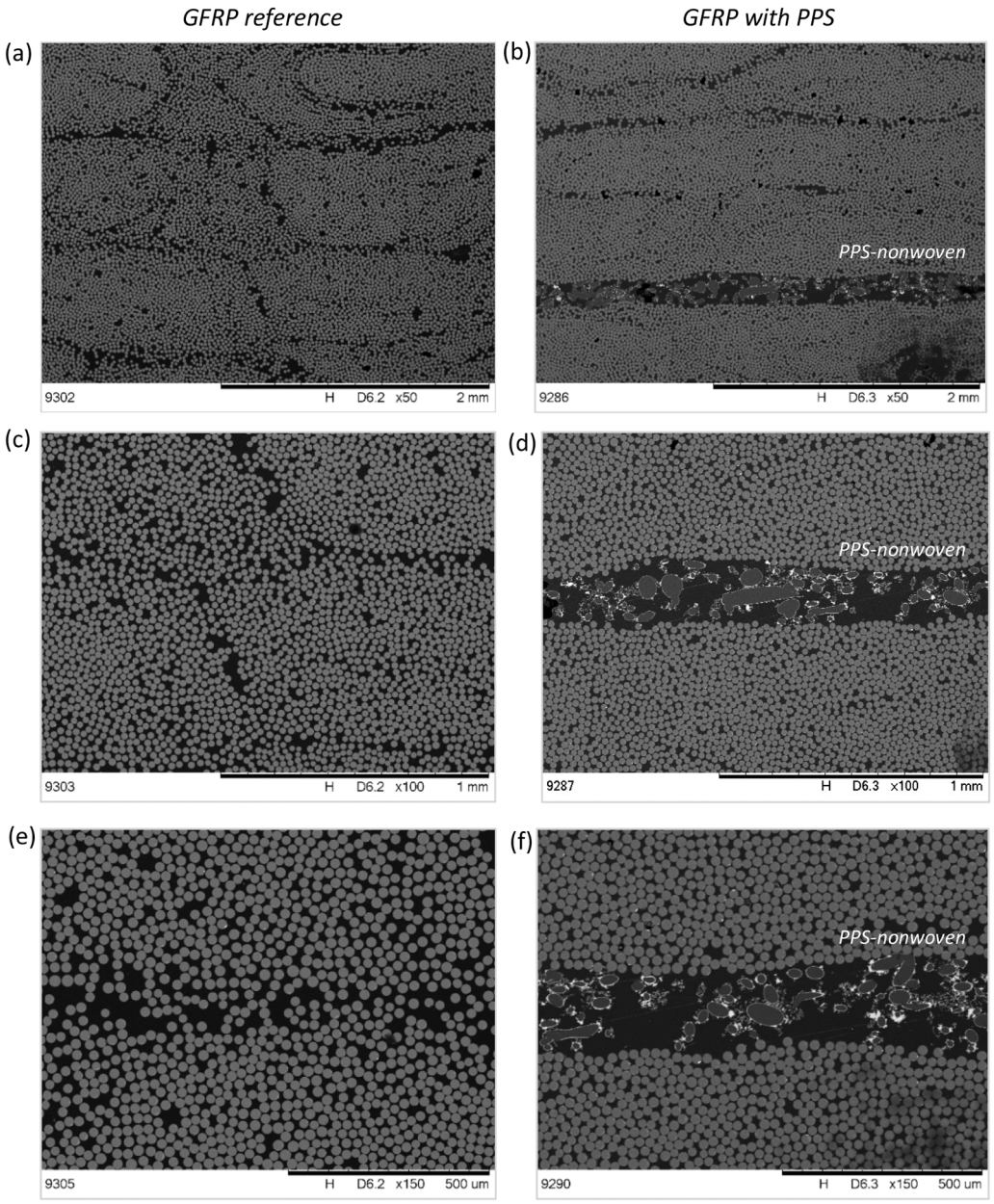

Fig. 7. Cross- sections of GFRP panels without metallized PPS nonwoven layer (a, c, e) and GFRP panels containing metallized PPS nonwoven layer (b,d, f).

(halogen lamps). The shearography inspection results were similar for the GFRP specimens with and without the PPS layer (Fig. 11 c-d). The vertical and diagonal lines in Fig. 11 c-d indicate the composite layup. These observations show that the PPS interlayer did not introduce structural defects that could act as artificial damage sources in shearography; therefore, the signals detected after the subsequent impact tests can be attributed to actual impact-induced damage.

Two GFRP specimens (called A and B), both containing metallized PPS-nonwovens, were examined in the shearography test. Fig. 12 a and b shows the shearography inspection results for specimen A before and after the impact test. The signature of impact damage is clear in the cooling state of the specimen (Fig. 12b). Fig. 12c and d represents the shearography inspection results for specimen B before and after impact test, where the impact damage was also detected during the cooling state (Fig. 12d). The impact damage in specimen B (along with delamination, and potential fiber breakage and matrix cracking) appears more pronounced than in specimen A. This difference is due to the randomly distributed fibers in the nonwovens. Therefore, although the same type of PPS nonwoven was used in specimens A and B, the resulting heating patterns are not identical, even though the heating time was kept constant at 240 s.

In the present study, we utilized the self-heating capability of the PPS nonwoven layer as a convenient means of applying thermal loading as an alternate to applying external heating. The metallized PPS nonwovens offer a lightweight and integrable solution, reducing the need for separate heating elements and enabling a more compact experimental setup.

3.5. *Effect of metallized nonwoven on the GFRP' mechanical properties*

The flexural behaviour of the analyzed laminates is presented in Fig. 13, which shows a clear difference between the reference composite and the material modified with the metalized PPS-based nonwoven. The reference laminate achieved a flexural modulus of approximately 40.6 GPa and a flexural strength of nearly 944 MPa, whereas the introduction of the metalized PPS interlayer increased these values to

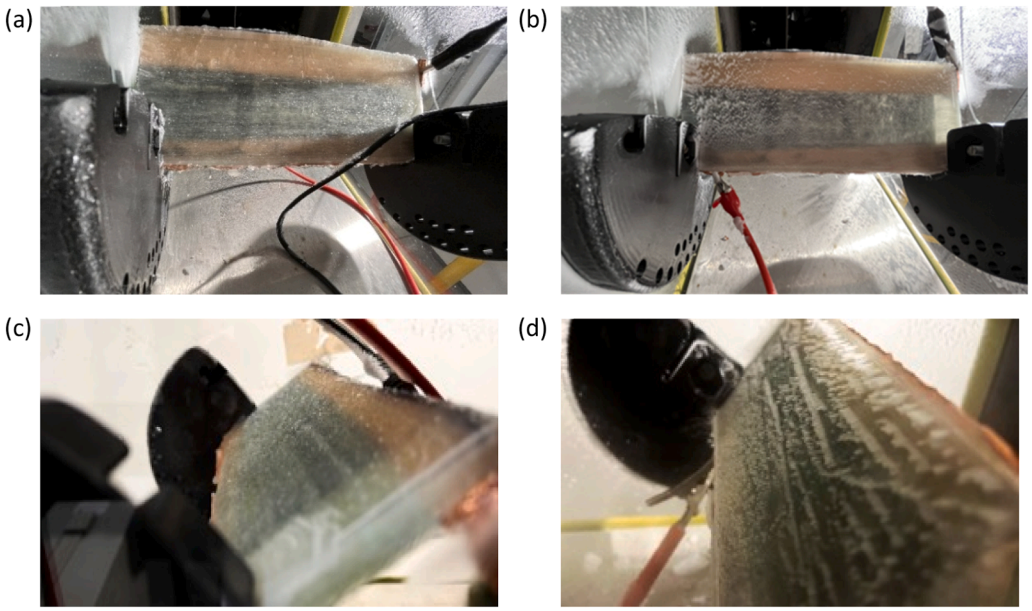

Fig. 8. GFRP specimens after ice accretion: (a) and (c) show glaze ice regime from different angle orientations; (b) and (d) show mixed ice regime from different angle orientations.

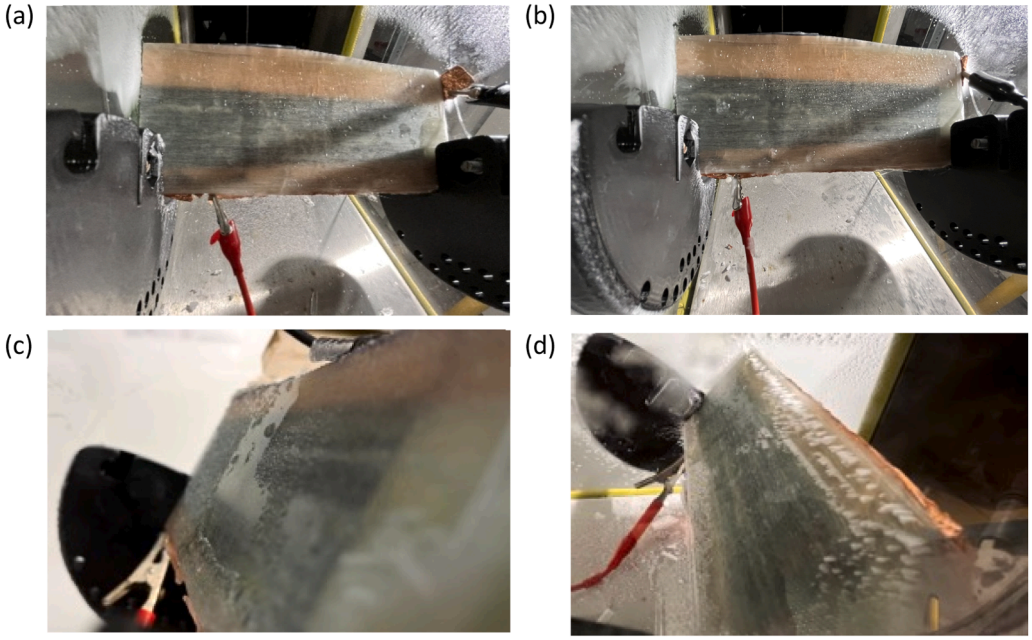

Fig. 9. GFRP specimens after 120 s of power activation: (a) and (c) show glaze ice from different angle orientations; (b) and (d) show mixed ice from different angle orientations.

around 43.4 GPa and 1164 MPa. The shift observed on the plot indicates that the additional layer predominantly affects the region associated with damage onset, as the elastic response remains governed mainly by the glass-fiber architecture. In contrast, the PPS structure appears to become active once the material approaches the initiation of micro-cracking. This behaviour is consistent with the role of tailored interlayers in fiber-reinforced laminates, which can redistribute local stresses during bending and delay the propagation of early damage, thereby allowing the laminate to carry higher loads before failure. The more pronounced increase in flexural strength relative to stiffness suggests that the interlayer primarily influences the mechanisms responsible for crack formation rather than altering the overall elastic response of the composite. Similar relationships for interleaved fiber-reinforced laminates were also reported by de Souza and Tarpani [33].

The results of the DMA analysis are presented in Fig. 14. The storage modulus (E') curves show that both materials exhibit similar stiffness in the glassy region, with values of 24.3 GPa for the reference GFRP and 25.9 GPa for the modified one. The slight increase in E' at room temperature suggests that the presence of the stiff interlayer of metallized PPS-nonwovens marginally reinforces the GFRP and restricts local deformation in the elastic regime, which is consistent with reports showing that rigid secondary phases can enhance composite stiffness [34]. A clear difference was observed in the temperature dependence of both E' and tangens delta (tan δ). The glass transition temperature, determined from the tan δ peak, shifts from 132 °C for the reference GFRP to 141 °C for the laminate containing the metallized nonwoven.

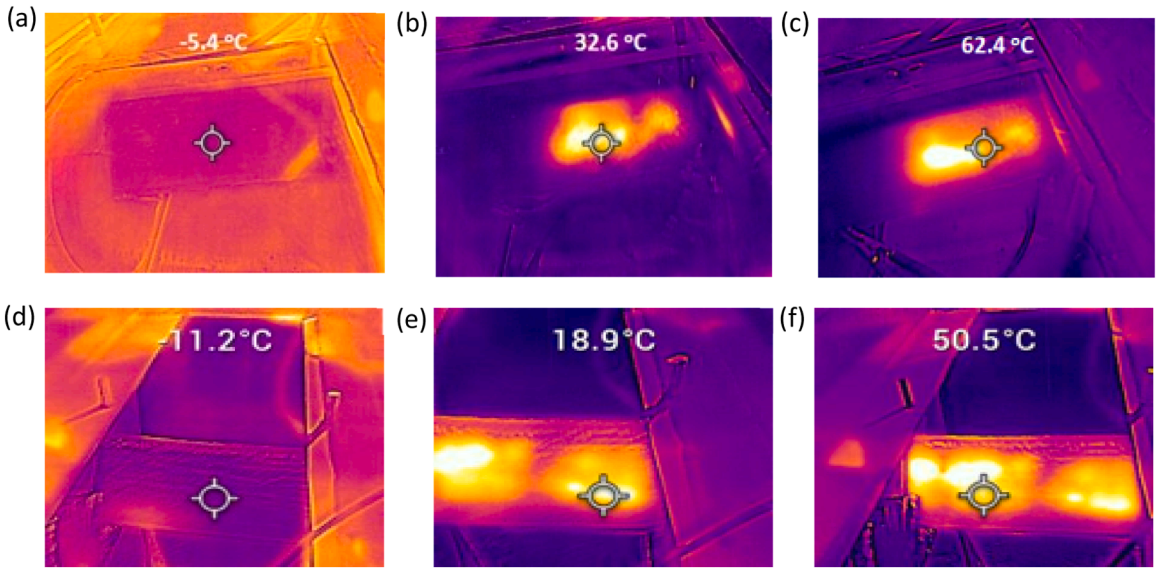

Fig. 10. Surface temperature evolution of GFRP samples under icing conditions: (a–c) glaze ice regime after (a) 0 s, (b) 30 s, (c) 120 s of power activation; (d–f) mixed ice regime after (d) 0 s, (e) 30 s, (f) 120 s of power activation.

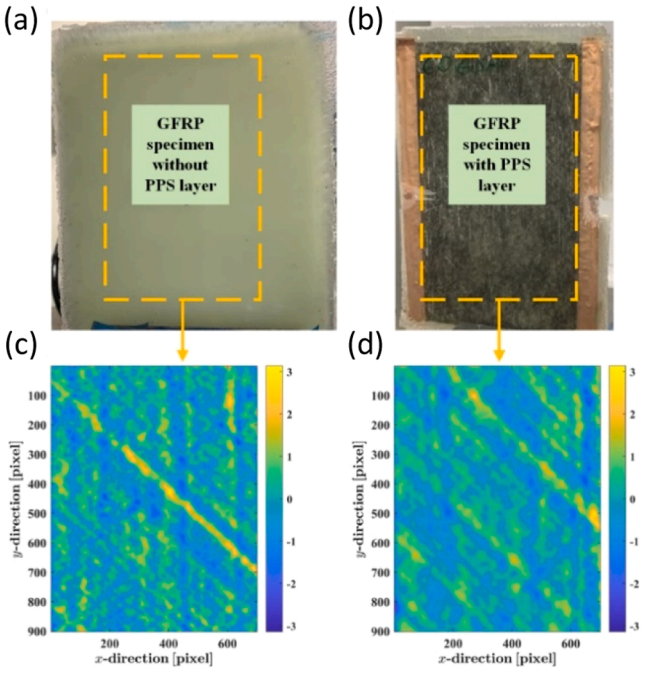

Fig. 11. Preliminary shearography tests on GFRP specimens without and with a PPS layer. (a) Photo of the GFRP specimen without PPS layer. (b) Photo of the GFRP specimen with a PPS layer. (c) The shearography result on the GFRP specimen without PPS layer. (d) The shearography result on the GFRP specimen with a PPS layer.

This shift coincides with a corresponding displacement of the E′ drop toward higher temperatures, indicating reduced segmental mobility in the modified system. Similar increases in T_g have been reported in composites where stiff interphases or rigid fillers restrict polymer-chain motion and delay relaxation processes [35]. In addition, the value of the tan δ peak decreases considerably (0.70 → 0.42), indicating reduced molecular mobility and lower damping capacity in the modified laminate. In the present case, both the PPS nonwoven structure and the Ni–P coating may contribute to a locally constrained interphase, thereby suppressing segmental motion and increasing the effective T_g. The results obtained are consistent with those of the three-point bending test presented in [35] where the addition of metallized nonwoven fabric increased the stiffness and flexural strength of GFRP.

4. Conclusions

The study demonstrates the effective integration and multifunctional performance of metallized PPS nonwovens as electrically conductive interlayers in GFRP composites. Electroless Ni–P plating yielded a uniform metallic coating, as confirmed by EDS, while preserving the fibrous architecture of the nonwoven. The incorporation of metallized PPS nonwoven into the GFRP structure did not negatively affect the overall composite quality, confirming the effective integration of the heating layer, which enables the achievement of three key functionalities:

- The system provided efficient and reliable de-icing under representative icing conditions. In both glaze- and mixed-ice regimes, complete ice removal was achieved within approximately 120 s. The nonwoven architecture enabled distributed Joule heating, providing uniform temperature distribution and improved energy efficiency compared to localized heating systems.
- The metallized PPS nonwovens functioned as an internal thermal loading element to assist shearography NDT. The heat generated by the embedded layer enabled clear detection of impact-induced damage, including delamination and subsurface matrix crack, demonstrating the system's potential for the detection of impact-induced damage using this NDT technique.
- The incorporation of the metallized PPS interlayer did not deteriorate the mechanical properties of the composite. On the contrary, an increase in flexural strength (from 944 MPa to approximately 1164 MPa) and a slight increase in glass transition temperature (from 132 °C to 141 °C) were observed.

From a practical perspective, metallized PPS nonwovens offer a lightweight, integrable solution combining heating and sensing functionalities within a single interlayer, reducing the need for separate heating elements and enabling a more compact experimental setup. This approach is particularly advantageous for composite structures operating under icing conditions, where both efficient de-icing and structural health monitoring are required.

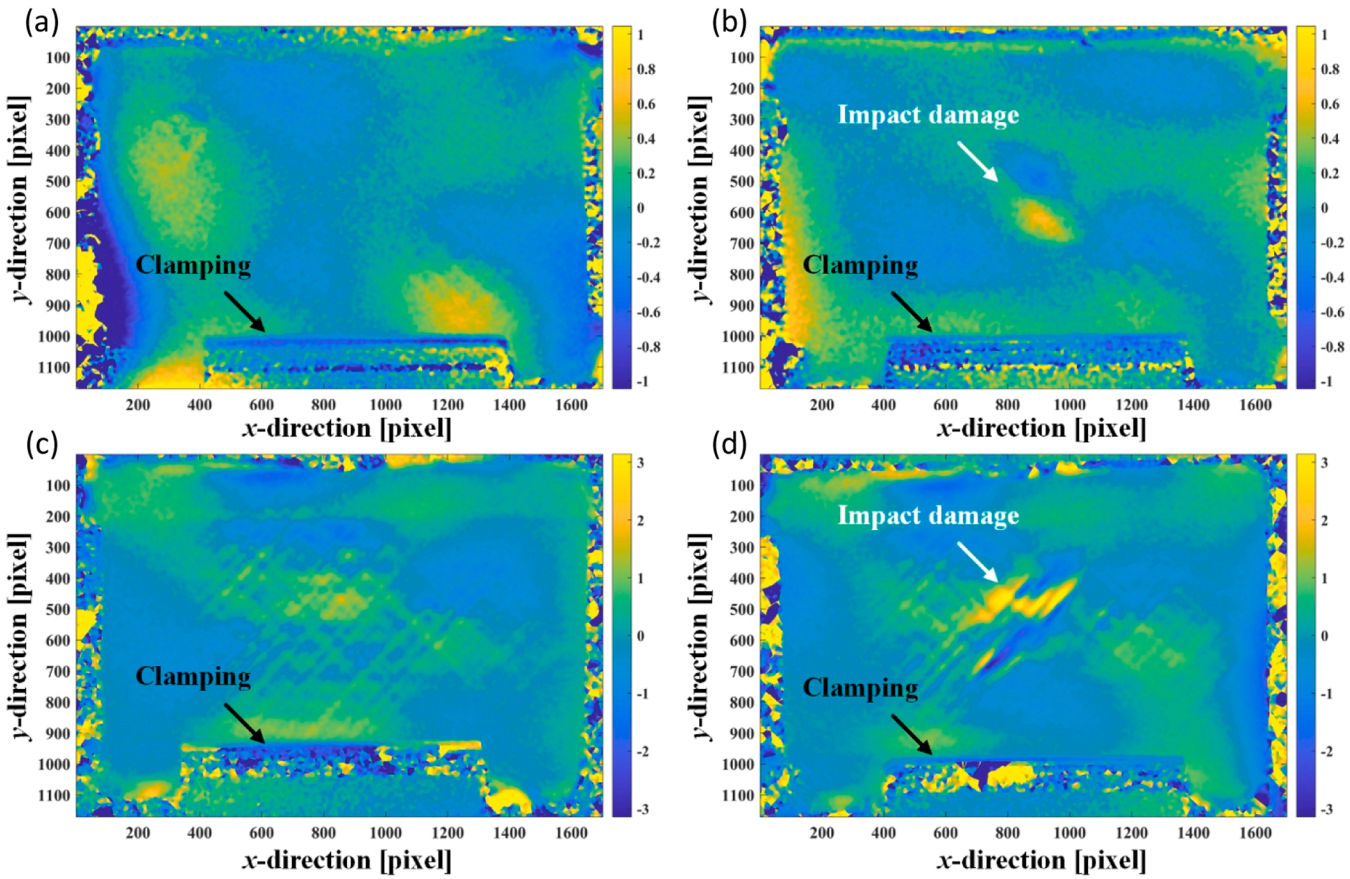

Fig. 12. Shearography results: (a) GFRP A - cooling state, before impact. (b) GFRP A- cooling state, after impact.(c) GFRP B - cooling state, before impact. (d) GFRP B – cooling state, after impact. Shearing direction in the y axis (vertical).

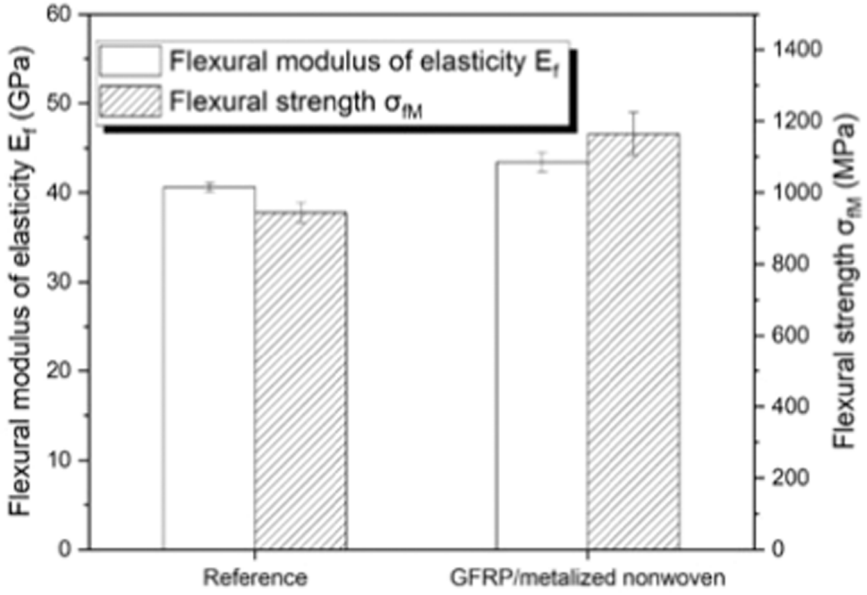

Fig. 13. The effect of metallized PPS-nonwoven integration on flexural properties of GFRP composites.

CRediT authorship contribution statement

Otto Bergsma: Validation, Supervision, Funding acquisition, Formal analysis. **Paweł Durałek:** Methodology, Investigation, Conceptualization. **Daria Rutkowska:** Writing – original draft, Software, Methodology, Investigation. **Milena Kurkowska:** Validation, Supervision, Methodology. **Andrei Anisimov:** Validation, Supervision, Methodology. **Michał Misiak:** Visualization, Software, Methodology, Investigation. **Dola Temesgen Ufaysa:** Writing – original draft, Visualization, Methodology, Investigation. **Nan Tao:** Writing – original

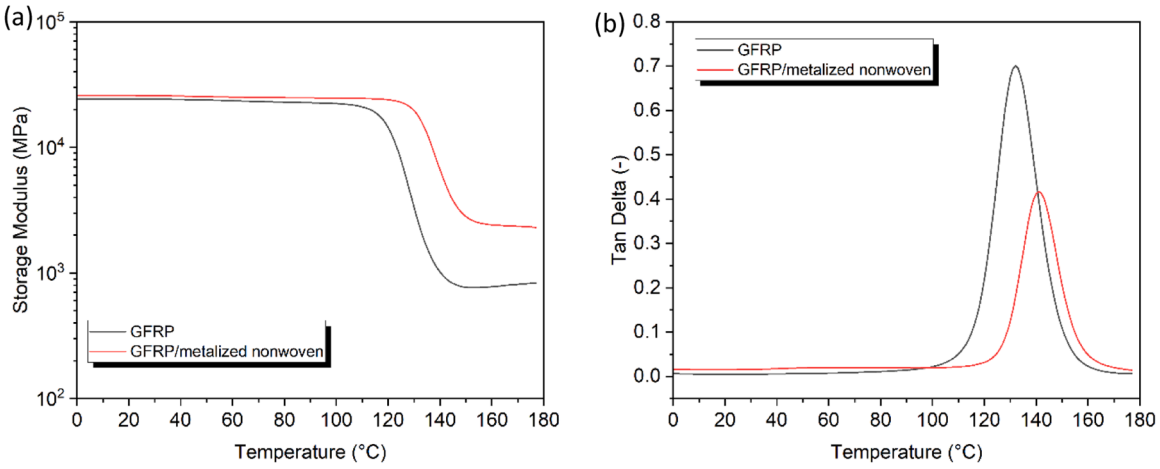

Fig. 14. (a) Storage modulus and (b) tan δ of reference GFRP and GFRP with metalized nonwoven.

draft, Visualization, Software, Methodology, Investigation. **Bartłomiej Przybyszewski:** Writing – original draft, Software, Methodology, Investigation. **Roger M. Groves:** Validation, Supervision, Project administration, Formal analysis. **Paulina Latko-Durałek:** Writing – original draft, Investigation, Formal analysis, Data curation, Conceptualization. **Anna Boczkowska:** Supervision, Project administration, Funding acquisition.

Declaration of Competing Interest

The authors declare that they have no known competing financial interests or personal relationships that could have appeared to influence the work reported in this paper.

Acknowledgement

The work presented in this paper has been carried out within the HORIZON-WIDERA-2021-ACCESS-03–01 - Twinning COMPECO project, co-funded by the European Commission (Project Number:101079250).

Data availability

Data will be made available on request.

References

[1] P. Latko-Durałek, P. Durałek, A. Boczkowska, R. Kozera, M. Wróblewska, A. Mazik, Characterization of thermoplastic nonwovens of copolyamide hot melt adhesives filled with carbon nanotubes produced by melt-blowing method, J. Ind. Text. 51 (2022) 1235S–1251S, https://doi.org/10.1177/1528083720910213.
[2] Y. Kara, K. Molnár, A review of processing strategies to generate melt-blown nano/microfiber mats for high-efficiency filtration applications, J. Ind. Text. 51 (2022) 137S–180S, https://doi.org/10.1177/15280837211019488.
[3] Applications of Nonwovens, in: Ra Chapman, Ra Chapman (Eds.), Technical Textiles, Woodhead Publishing, 2010. ⟨https://www.sciencedirect.com/book/edited-volume/9781845694371/applications-of-nonwovens-in-technical-textiles⟩.
[4] Gorjanc Dunja Sajn, Functional properties of nonwovens as an insulating layer for protective gloves, Polymers (2023) 785.
[5] Ö. Güzdemir, V. Bermudez, S. Kanhere, A.A. Ogale, Melt-spun poly(lactic acid) fibers modified with soy fillers: Toward environment-friendly disposable nonwovens, Polym. Eng. Sci. 60 (2020) 1158–1168, https://doi.org/10.1002/pen.25369.
[6] A.K.P. Dhanakodi, T. Hemamalini, A.B. Navamithra, T. Arun, G. Swetha, V.R. Giri Dev, Effect of carbon fillers as fibres on the flexural and impact performance of wet laid polypropylene nonwoven composites, J. Text. Inst. (2021), https://doi.org/10.1080/00405000.2021.1893483.
[7] J. Ziaja, J. Koprowska, J. Janukiewicz, Using plasma metallisation for manufacture of textile screens against electromagnetic fields, Fibres Text. East. Eur. 16 (2008) 64–66.
[8] J. Koprowska, E. Dobruchowska, K. Reszka, A. Szwugier, Morphology and electromagnetic shielding effectiveness of pp nonwovens modified with metallic layers, F. TinEE 23 (2015) 84–91, https://doi.org/10.5604/12303666.1161763.
[9] W. Qin, R. Guo, Metallization of polyester fabric by autocatalytic copper plating process using glyoxylic acid as a reducing agent, Fibers Polym. 16 (2015) 1671–1675, https://doi.org/10.1007/s12221-015-4943-4.
[10] E. Khajeh, K. Nasouri, G. Askari, M. Mandegari, Flexible and lightweight metalized polyamide nonwoven for electromagnetic interference shielding, electrothermal, photothermal, and antibacterial applications, Chem. Eng. J. 502 (2024) 158203, https://doi.org/10.1016/j.cej.2024.158203.
[11] M. Bai, J. Wang, R. Zhou, Z. Lu, L. Wang, X. Ning, Polyphenylene sulfide fabric with enhanced oxidation resistance and hydrophobicity through polybenzoxazine surface coating for emission control in harsh environment, J. Hazard. Mater. 432 (2022) 128735, https://doi.org/10.1016/j.jhazmat.2022.128735.
[12] X. Tang, X. Zhao, Y. Lu, S. Li, Z. Zhang, M. Zhu, K. Yao, J. Zheng, H. Chen, Y. Duan, Y. Qiao, Z. Wang, T. Liu, Flexible metalized polyimide nonwoven fabrics for efficient electromagnetic interference shielding, Chem. Eng. J. 480 (2024) 148000, https://doi.org/10.1016/j.cej.2023.148000.
[13] S. Reich, M. Burgard, M. Langner, S. Jiang, X. Wang, S. Agarwal, B. Ding, J. Yu, A. Greiner, Polymer nanofibre composite nonwovens with metal-like electrical conductivity, Npj Flex. Electron 2 (2018) 5, https://doi.org/10.1038/s41528-017-0018-5.
[14] R. Rekuviene, S. Saeidiharzand, L. Mažeika, V. Samaitis, A. Jankauskas, A. K. Sadaghiani, G. Gharib, Z. Muganlı, A. Koşar, A review on passive and active anti-icing and de-icing technologies, Appl. Therm. Eng. 250 (2024) 123474, https://doi.org/10.1016/j.applthermaleng.2024.123474.
[15] E. Esmaeilifar, L. Prince Raj, R.S. Myong, Computational simulation of aircraft electrothermal de-icing using an unsteady formulation of phase change and runback water in a unified framework, Aerosp. Sci. Technol. 130 (2022) 107936, https://doi.org/10.1016/j.ast.2022.107936.
[16] Aleksei V. Shiverskii, Mohammad Owais, Biltu Mahato, Sergey G. Abaimov, Electrical Heaters for Anti/De-Icing of Polymer Structures, Polymers (2023), https://doi.org/10.3390/polym15061573.
[17] X. Guo, Q. Yang, H. Zheng, W. Dong, Integrated composite electrothermal de-icing system based on ultra-thin flexible heating film, Appl. Therm. Eng. 236 (2024) 121723, https://doi.org/10.1016/j.applthermaleng.2023.121723.
[18] J. Lee, H. Jo, H. Choe, D. Lee, H. Jeong, H. Lee, J. Kweon, H. Lee, R. Shin Myong, Y. Nam, Electro-thermal heating element with a nickel-plated carbon fabric for the leading edge of a wing-shaped composite application, Compos. Struct. 289 (2022) 115510, https://doi.org/10.1016/j.compstruct.2022.115510.
[19] A.V. Shchegolkov, A.V. Shchegolkov, V.V. Kaminskii, P. Iturralde, M.A. Chumak, Advances in electrically and thermally conductive functional nanocomposites based on carbon nanotubes, Polymers 17 (2025) 71, https://doi.org/10.3390/polym17010071.
[20] B. Zheng, H. Wang, X. Wu, K. Yang, Y. Yu, H. Cui, F. Gao, K. Qian, H. Yao, J. Li, W. Xu, X. Gong, Y. Wang, Z. Zhang, Y. Dong, Flexible nanocomposite electrothermal films based on carbon nanotubes and waterborne polyurethane with high reliability, stretchability and low-temperature performance for wind turbine blade deicing, Compos. Part A Appl. Sci. Manuf. 158 (2022) 106979, https://doi.org/10.1016/j.compositesa.2022.106979.
[21] M. Al-Bahrani, J. Graham-Jones, Z. Gombos, A. Al-Ani, A. Cree, High-efficient multifunctional self-heating nanocomposite-based MWCNTs for energy applications, Int. J. Energy Res. 44 (2020) 1113–1124, https://doi.org/10.1002/er.4999.
[22] R. Groves, Inspection and Monitoring of Composite Aircraft Structures, Ref. Modul. Mater. Sci. Mater. Eng. (2017), https://doi.org/10.1016/B978-0-12-803581-8.10340-6.
[23] D. Francis, R.P. Tatam, R.M. Groves, Shearography technology and applications: a review, Meas. Sci. Technol. 21 (2010) 102001, https://doi.org/10.1088/0957-0233/21/10/102001.

[24] W. Steinchen, L.X. Yang. Digital shearography: theory and application of digital speckle pattern shearing interferometry, SPIE Press, Bellingham, WA, USA, 2003.
[25] J. Newman, Shearography Nondestructive Testing of Composites, Ref. Modul. Mater. Sci. Mater. Eng. (2017), https://doi.org/10.1016/B978-0-12-803581-8.10046-3.
[26] N. Tao, A.G. Anisimov, R.M. Groves, Shearography non-destructive testing of thick GFRP laminates: Numerical and experimental study on defect detection with thermal loading, Compos. Struct. 282 (2022) 115008, https://doi.org/10.1016/j.compstruct.2021.115008.
[27] N. Tao, R.M. Groves, A.G. Anisimov, Shearography pair method for reliable non-destructive inspection of millimeter and submillimeter defects in fiber-reinforced composites, Measurement 255 (2025) 117980, https://doi.org/10.1016/j.measurement.2025.117980.
[28] A.G. Anisimov, M.G. Serikova, R.M. Groves, 3D shape shearography technique for surface strain measurement of free-form objects, Appl. Opt. AO 58 (2019) 498–508, https://doi.org/10.1364/AO.58.000498.
[29] Research offer – Icing Wind Tunnel, (n.d.). ⟨https://icingwindtunnel.pl/research-offer/⟩ (accessed December 15, 2025).
[30] N. Tao, A.G. Anisimov, R.M. Groves, FEM-assisted shearography with spatially modulated heating for non-destructive testing of thick composites with deep defects, Compos. Struct. 297 (2022) 115980, https://doi.org/10.1016/j.compstruct.2022.115980.
[31] Z.A. Janjua, B. Turnbull, S. Hibberd, K.-S. Choi, Mixed ice accretion on aircraft wings, Phys. Fluids 30 (2018) 027101, https://doi.org/10.1063/1.5007301.
[32] M. Yamazaki, A. Jemcov, H. Sakaue, A Review on the Current Status of Icing Physics and Mitigation in Aviation, Aerospace 8 (2021) 188, https://doi.org/10.3390/aerospace8070188.
[33] G. de Souza, J.R. Tarpani, Interleaving CFRP and GFRP with a Thermoplastic Ionomer: The Effect on Bending Properties, Appl. Compos. Mater. 28 (2021) 559–572, https://doi.org/10.1007/s10443-021-09874-2.
[34] G. Anand, N. Alagumurthi, R. Elansezhian, N. Venkateshwaran, Dynamic mechanical, thermal and wear analysis of Ni-P coated glass fiber/Al_2O_3 nanowire reinforced vinyl ester composite, Alex. Eng. J. 57 (2018) 621–631, https://doi.org/10.1016/j.aej.2017.02.013.
[35] M. Landowski, M. Budzik, K. Imieli'nska, Dynamic mechanical behaviour of GFRP composites with SiO2 nano particles reinforced Epoxy matrix, Adv. Mater. Sci. 13 (2013) 5–8, https://doi.org/10.2478/adms-2013-0014.